Temporal scaling of human scalp-recorded potentials

Cameron D. Hassall, Jack Harley, Nils Kolling, and Laurence T. Hunt*

Oxford Centre for Human Brain Activity, Wellcome Centre for Integrative Neuroimaging, Department of Psychiatry, University of Oxford, Oxford OX3 7JX, United Kingdom

*laurence.hunt@psych.ox.ac.uk

Abstract

Much of human behaviour is governed by common processes that unfold over varying timescales. Standard event-related potential analysis assumes *fixed-latency* responses relative to experimental events. However, recent single unit recordings in animals have revealed neural activity *scales* to span different durations during behaviours demanding flexible timing. Here, we employed a general linear modelling approach using a novel combination of fixed-duration and variable-duration regressors to unmix fixed-time and scaled-time components in human magneto/electroencephalography (M/EEG) data. We use this to reveal consistent temporal scaling of human scalp-recorded potentials across four independent EEG datasets, including interval perception, production, prediction and value-based decision making. The topography of these potentials is consistent with a source in medial frontal cortex, as studied in animal recordings. Between-trial variation in the temporally scaled response predicts between-trial variation in subject reaction times, demonstrating the relevance of this temporally scaled signal for temporal variation in behaviour. Our results provide a general approach for studying flexibly timed behaviour in the human brain.

Action and perception in the real world require flexible timing. We can walk quickly or slowly, recognize the same piece of music played at different tempos, and form temporal expectations over long and short intervals. In many cognitive tasks, reaction time variability is modelled in terms of internal evidence accumulation [1], whereby the same dynamical process unfolds at different speeds on different trials.

Flexible timing is critical in our lives, yet despite several decades of research [2–5] its neural correlates remain subject to extensive debate. Due to their high temporal resolution, magnetoencephalography and electroencephalography (M/EEG) have played a particularly prominent role in understanding the neural basis of timing [5–13], and the method typically used to analyze such data has been the event-related potential (ERP), which averages event-locked responses across multiple repetitions. For example, this approach has been used to show that the slope of a ramping frontal-central ERP component called the contingent negative variation (CNV) [14] depends inversely on the duration of the timed interval [7,8,12].

Crucially, the ERP analysis strategy implicitly assumes that neural activity occurs at *fixed-time* latencies with respect to experimental events. However, it has recently been shown that brain activity at the level of individual neurons can be best explained by a *temporal scaling* model [15,16], in which activity is explained by a single response that is stretched or compressed according to the length of the produced interval. When monkeys are cued to produce intervals of different lengths, the temporal scaling model explains the majority of variance in neural responses from medial frontal cortex (MFC) single units [15]. This suggests that one mechanism by which flexible motor timing can be achieved is by adjusting the speed of a common neural process, a perspective readily viewed through the lens of dynamical systems theory [16]. Consistent with the broad role played by dynamical systems in a range of neural computations [17,18], recent studies in neural populations have revealed

time-warping as a common property across many different population recordings and behavioural tasks [19]. For example, temporal scaling is also implicit in the neural correlates of evidence integration during sensory and value-based decision making [20] (which itself has also been proposed as a mechanism for time estimation in previous work [21]).

Successfully characterising scaled-time components in humans could open the door to studying the role of temporal scaling in more complex, hierarchical tasks such as music production or language perception, as well as in patient populations in which timing is impaired [22]. Yet it is currently unclear how temporal scaling of neural responses may manifest at the scalp (if at all) using non-invasive recording in humans. This is because of the fixed-time nature of the ERP analysis strategy. Again, one component of the ERP called the CNV has been found to ramp at different speeds for different temporal intervals [7,8,12], suggestive of temporal scaling. Crucially though, any scaled activity would appear mixed at the scalp with fixed-time components due to the *superposition problem* [23].

We therefore developed an approach to *unmix* scaled-time and fixed-time components in the EEG (Fig 1a). Our proposed method builds on recently developed least square regression-based approaches [24–29] that have proven useful in unmixing fixed-time components that overlap with one another, such as stimulus-related activity and response-related activity. To overcome the superposition problem, these approaches use a convolutional general linear model (GLM) to deconvolve neural responses that are potentially overlapping. Following this work, we estimate the fixed-time ERPs using a GLM in which the design matrix is filled with time-lagged dummy variables (1s around the events of interest, 0s otherwise). Importantly, these 'stick functions' can overlap in time to capture overlap in the underlying neural responses (Fig 1b), and the degree of fit to neural data can be improved by adding a regularisation penalty to the model estimation [29]. In situations without any overlap, the GLM would exactly return the conventional ERP.

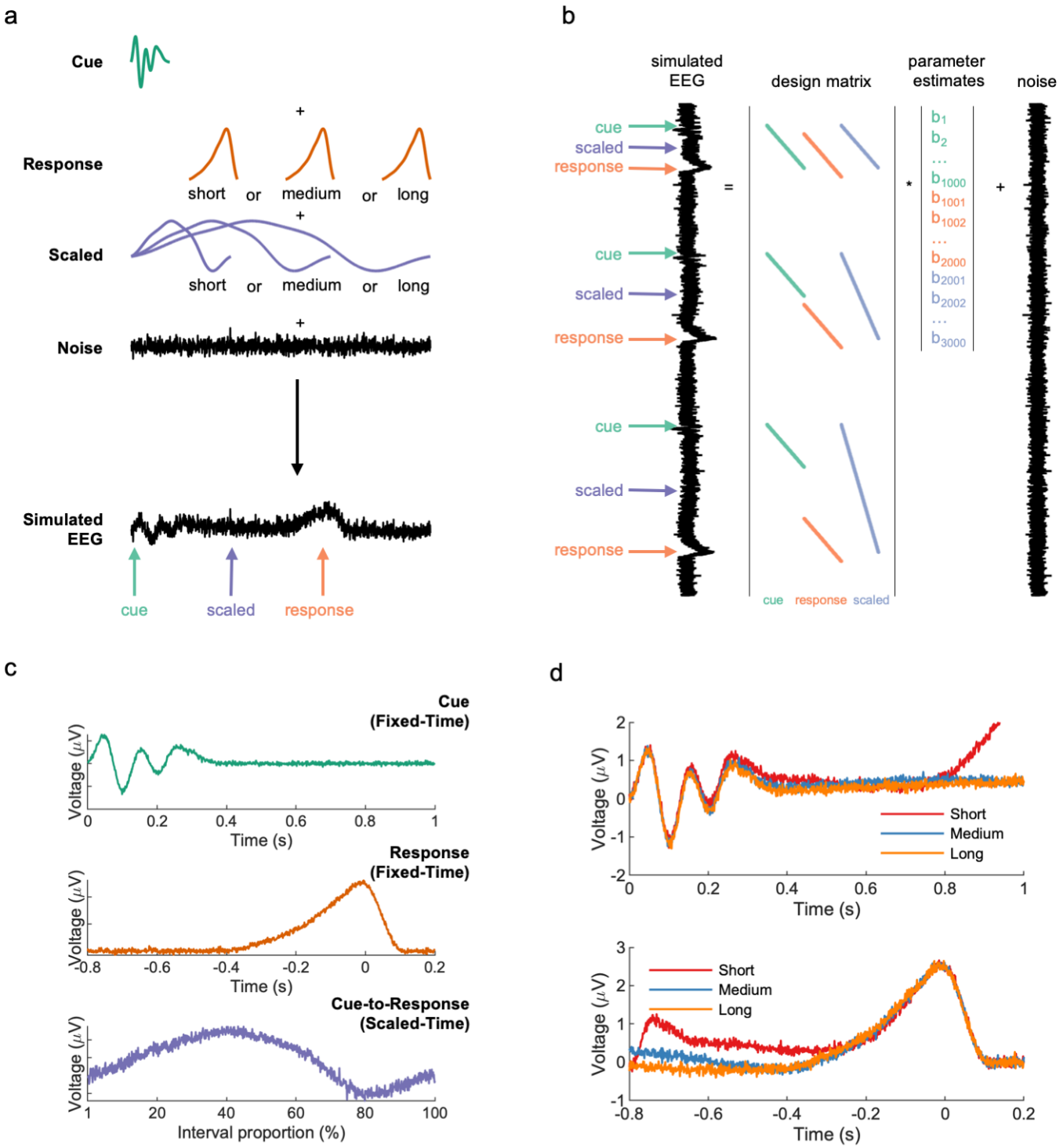

Fig 1. Regression based unmixing of simulated data successfully recovers scaled-time and fixed-time components. (a) EEG data were simulated by summing fixed-time components (cue and response), a scaled-time component with differing durations for different trials (short, medium, or long), and noise. (b) The simulated responses were unmixed via a GLM with stick basis functions: cue-locked, response-locked, and a single scaled-time basis spanning from cue to response. (c) The GLM successfully recovered all three components, including the scaled-time component. (d) A conventional ERP analysis (cue-locked and response-locked averages) of the same data obscured the scaled-time component.

The key innovation that we introduce here is to allow for *variable-duration* regressors in such models, in addition to fixed-duration regressors, to test for the presence of scaled-time

responses. In particular, we allow the duration of the stick function to vary depending upon the interval between stimulus and response, meaning that the same neural response can span different durations on different trials. We use a 'box-shaped' kernel to perform this interpolation, although we find that other interpolation methods produce similar results (Supplementary Fig 1). The returned scaled-time potential is no longer a function of real-world ('wall clock') time, but instead a function of the *percentage of time elapsed* between stimulus and response.

As a proof of concept, we simulated data at a single EEG sensor for an interval timing task, consisting of two *fixed-time components* (locked to cues and responses), and one *scaled-time component* spanning between cues and responses (Fig 1a). Our proposed method was successful in recovering all three components (Fig 1c), whereas a conventional ERP approach obscured the scaled-time component (Fig 1d). Crucially, in real EEG data we repeated this approach across all sensors, potentially revealing different scalp topographies (and hence different neural sources) for fixed-time versus scaled-time components.

We note that a time-frequency decomposition might also readily separate the responses at higher and lower-frequencies. Indeed, a wide range of neural oscillations have been implicated in time perception [30]. One might reasonably expect stretched/compressed signals to manifest differently in the time-frequency domain, e.g., as they correlate more strongly with different stretched/compressed versions of the same wavelet function. Unlike our proposed approach, however, a time-frequency decomposition is not readily designed to look for temporal scaling of the scaled-time response, namely the *same* neural response unfolding over *different* timescales on different trials. Nor will a time-frequency decomposition separate fixed-time responses from scaled-time responses if the signals occupy the same frequency band [31].

We used our approach to analyze EEG recorded across four independent datasets, comprising three interval timing tasks and one decision-making task. In the first task, participants produced a target interval (short, medium, or long) following a cue (Supplementary Fig 2a). Feedback was provided, and participants were able to closely match the target intervals (Supplementary Fig 3a). In the second, participants evaluated a computer-produced interval (Supplementary Fig 2b). The closer the produced interval was to the target interval, the more likely participants were to judge the response as 'on time' (Supplementary Fig 3b). In the third (previously analyzed [32,33]) task, participants made temporal predictions about upcoming events based on rhythmic predictions. In the fourth task (also previously analyzed [34,35]) participant chose between pairs of snack items – a process in which reaction time variability can be modelled as a process of internal evidence accumulation across time [36].

In all four tasks, we observed a scaled-time component that was distinct from the preceding and following fixed-time components (Fig 2), which resembled conventional ERPs (Supplementary Fig 4). Typically, ERP components are defined by their polarity and scalp distribution [37]. The observed scaled-time components shared a common polarity (negative) and scalp distribution (central), which is notably consistent with the medial frontal recording

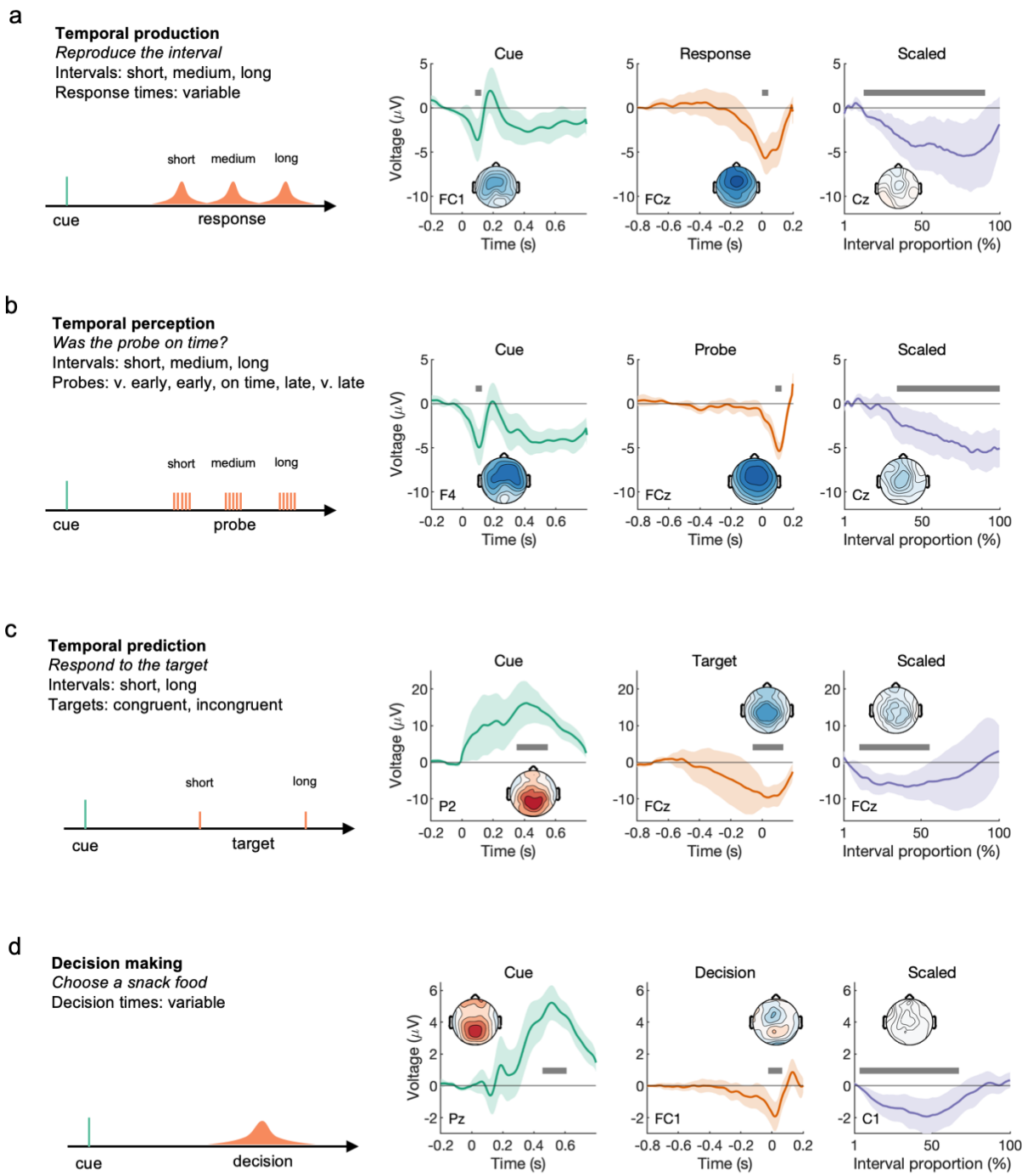

Fig 2. Scaled-time components were consistently observed across three time-estimation paradigms and one decision-making paradigm, with distinct scalp topographies from fixed-time components. Data were analyzed from: (a) a temporal production task; (b) a temporal judgement task; (c) a temporal prediction task[11,12]; (d) a decision-making task[13,14]. All had distinct fixed-time components relative to task-relevant events (left/middle columns), and a common negative scaled-time component over central electrodes, reflecting interval time (right column). The scalp topographies represent the mean voltage across the intervals indicated by the grey bars. For the fixed-time components, the intervals were chosen to visualize prominent deflections in the average waveform. For the scaled-time components, the intervals represent regions of significance as determined by cluster-based permutation tests. The error bars represent 95% confidence intervals.

site where temporally scaled single-unit responses were previously identified [15]. In each task, cluster-based permutation testing revealed that the scaled-time component differed

significantly from zero. The differences were driven by clusters spanning 13-91% in the production task (p = .01), 34-100% in the perception task (p = .001), 11-56% in the prediction task (p = .004), and 4-68% in the decision-making task (p = .01). In many cases, scaled-time components were reliably observed at the single-subject level (Supplementary Fig 4-7).

We then examined how the scaled-time component related relates to behavioural variability: does the latency of the scaled-time component predict participants' response time? We focussed on the temporal production and decision-making tasks, in which the scaled-time component spanned the duration from cue to response. To measure component latency, we applied an approach developed in [38,39], using principal component analysis (PCA) to model delay activity over central electrodes in the temporal production task, after first regressing out fixed-time components from the data (Fig 3a-c). PCA was applied separately to each of three produced intervals. This consistently revealed a first principal component that matched the shape of the scaled-time component and a second principal component that matched its *temporal derivative*. This analysis confirms the presence of the scaled-time component in our data, as it is the first principal component of the residuals after removing fixed-time components. Crucially, adding or subtracting the second principal component captures variation in the *latency* of the scaled-time component (Supplementary Fig 5). Across response time quantiles, we found that PC2 scores (Supplementary Table 3) were significantly related to response times (Fig 3d), $F(2,18) = 8.31$, $p = .003$, $\eta_p^2 = 0.48$, $\eta_g^2 = 0.43$). This implies that the earlier in time that the scaled-time component peaked, the faster

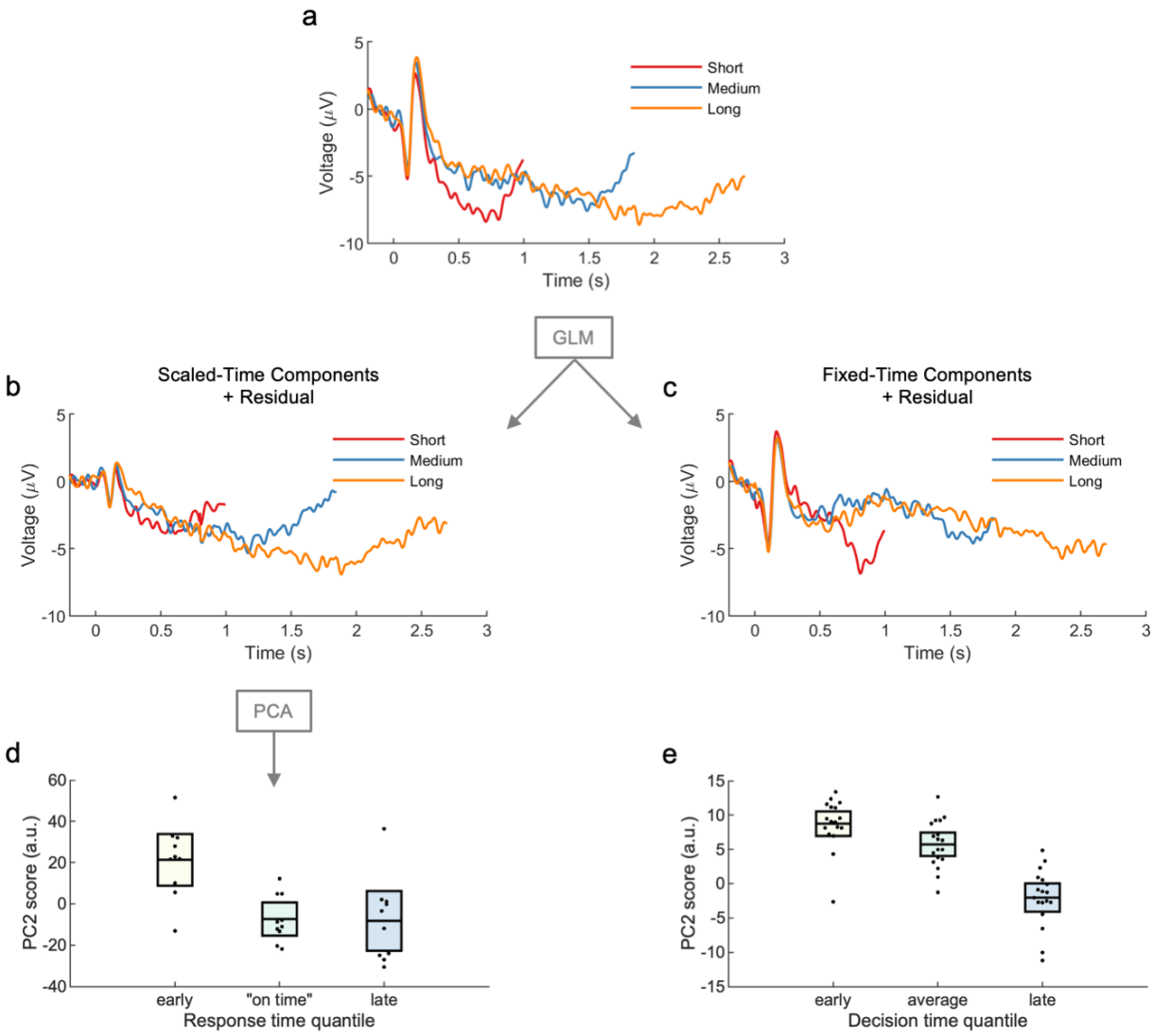

Fig 3. Variation in scaled-time components predicts behavioural variation in time estimation. Cue-locked EEG, shown as ERPs in (a), was analyzed via GLM. To visualize the unmixing of scaled-time and fixed-time components, the residual (noise) was recombined with either the scaled-time component (b) or the fixed-time components (c). PCA was run on the 'scaled-time plus residual' EEG. The second principal component resembled the temporal derivative or 'rate' of the scaled component (Supplementary Fig 5). (d) PC2 scores depended on response time, implying the scaled-time component peaked earlier for fast responses and later for slow responses. (e) The effect replicated in a decision-making task. Error bars represent 95% confidence intervals.

the subject would respond on that trial. This result was replicated in the decision-making task, $F(2,34) = 43.60$, $p < .001$, $\eta_p^2 = 0.72$, $\eta_g^2 = 0.61$ (Fig 3e).

Discussion

Our results provide a general method for recovering temporally scaled signals in human M/EEG, where scaled-time components are mixed at the scalp with conventional fixed-time ERPs. We focused here on tasks that have been widely used in the timing literature, namely interval production, perception, and prediction, as well as an example of a

124 cognitive task that exhibits variable reaction times across trials (value-based decision
125 making). Distinct scaled-time components and scalp topographies were revealed in all four
126 tasks. These results suggest that flexible cognition relies on temporally scaled neural activity,
127 as seen in recent animal work [15,16].

128 The existence of temporally scaled signals at the scalp may not be surprising to those
129 familiar with the study of time perception. Because of its excellent temporal resolution, EEG
130 has long been used to study delay activity in interval timing tasks. As discussed, one signal of
131 interest has been a ramping frontal-central signal called the CNV, which we observed in our
132 conventional ERP analysis (Supplementary Fig 4). Notably, CNV slope has been interpreted
133 as an accumulation signal in pacemaker-accumulation models of timing [7,8,11,13]. Our
134 work differs from these previous studies in one important respect. In a conventional ERP
135 analysis, delay activity is assumed to occur over fixed latencies. The CNV is thus computed
136 by averaging over many cue-locked EEG epochs of the same duration. In contrast, we have
137 considered the possibility that scalped-recorded potentials reflect a mixture of both fixed-time
138 and scaled-time components. By modelling fixed-time and scaled-time components
139 separately, we revealed scaled activity that was common across all timed intervals. This, in
140 turn, is consistent with a recent class of models of timing that propose time estimation reflects
141 the variable speed over which an underlying dynamical system unfolds [16–18].

142 We also observed temporally scaled activity in a decision-making task, a somewhat
143 surprising result given that the task did not have an explicit timing component (participants
144 made simple binary decisions [34]). Nevertheless, time is the medium within which decisions
145 are made [40]. Computationally, the timing of binary decisions can be captured in a drift
146 diffusion model as the accumulation of evidence in favour of each alternative [1]. This
147 accumulation is thought to be indexed by an ERP component called the central parietal
148 positivity (CPP) [41]. There is evidence that the slope of the CPP – which can be either

stimulus-locked or response-locked – captures the rate of evidence accumulation [42]. For faster/easier decisions the CPP climbs more rapidly compared to slower/harder decisions [41,42]. Perhaps these effects can also be explained by stretching/compressing a common scaled-time component while holding stimulus- and response-related activity constant. Furthermore, variation in the scaled-time component is relevant to decision making according to our results: it predicts *when* a decision will be made. However, we also note that the topography observed in our scaled-time component was a negative-going potential rather than positive (Fig 2d). This can potentially be explained by the standard CPP-like ERP [34] being a mixture of our observed negative scaled-time topography with the positive fixed-time topographies.

Although we have focused here on interval timing and decision-making tasks, we anticipate other temporally-scaled EEG and MEG signals will be discovered for cognitive processes known to unfold over varying timescales. For example, the neural basis of flexible (fast/slow) speech production and perception is an active area of research [43–45], and may involve a form of temporal scaling [46]. Flexible timing is also important across a vast array of decision-making tasks, where evidence accumulation can proceed quickly or slowly depending on the strength of the evidence [20]. Flexible timing helps facilitate a range of adaptive behaviours via temporal attention [4], while disordered timing characterizes several clinical disorders [47], underscoring the importance of characterising temporal scaling of neural responses in human participants.

Acknowledgements

This research was funded by a Natural Sciences and Engineering Research Council of Canada (NSERC) Postdoctoral Fellowship to C.D.H., a BBSRC AFL Fellowship (BB/R010803/1) to N.K., a Sir Henry Dale Fellowship from the Royal Society and Wellcome (208789/Z/17/Z) to L.T.H., a NARSAD Young Investigator Award from the Brain and Behavior Research Foundation to L.T.H., and supported by the NIHR Oxford Health Biomedical Research Centre. The Wellcome Centre for Integrative Neuroimaging was supported by core funding from Wellcome Trust (203139/Z/16/Z). For the purpose of Open Access, the author has applied a CC BY public copyright licence to any Author Accepted Manuscript version arising from this submission.

Author Contributions

N.K. and L.T.H. conceived the experiments and methodology. C.D.H. and L.T.H. designed the experiments and developed the methodology. C.D.H. and J.H. performed the experiments (except for the prediction task, where data was downloaded from a previous publication [32,33]). C.D.H. and L.T.H. analyzed the data. C.D.H. and L.T.H. wrote the manuscript with input from the other authors.

Competing interests

The authors declare no competing interests.

Additional information

Supplementary information is available for this paper.

Correspondence and requests for materials should be addressed to L.T.H.

Methods

Simulations

We simulated cue-related and response-related EEG in a temporal production task using MATLAB 2020a (Mathworks, Natick, USA). Cue and response were separated by either a short, medium, or long interval. During the delay period, we simulated a scaled response that stretched or compressed to fill the interval. All three responses (cue, response, scaled) were summed together at appropriate lags (short, medium, or long), with noise – see Fig 1a. In total, we simulated 50 trials of each condition (short, medium, long).

To unmix fixed-time and scaled-time components, we used a regression-based approach [24,25,48] in which the continuous EEG at one sensor Y is modelled as a linear combination of the underlying event-related responses β, which are unknown initially. The model can be written in equation form as:

$$Y = X\beta + \varepsilon$$

where X is the design matrix and ε is the residual EEG not accounted for by the model. X contains as many rows as EEG data points, and as many columns as predictors (that is, the number of points in the estimated event-related responses). In our case, X was populated by 'stick functions' – non-zero values around the time of the modelled events, and zeros otherwise. We included in X two fixed-time components, the cue and the response, as stick functions of fixed EEG duration (with variables set to 1). In other words, the height of the fixed-time stick function was constant across events of the same type and equal to its width. To model a temporally-scaled response, we used the MATLAB *imresize* function (Image Processing Toolbox, R2020b) with 'box' interpolation to stretch/compress a stick function so that it spanned the duration between cue and response (other interpolation methods were tried – see Supplementary Fig 1 – but this choice had little effect on the results). Thus, the duration of the scaled stick function varied from trial to trial (Fig 1b). The

194 goal here was to estimate a single scaled-time response to account for EEG activity across
195 multiple varying delay periods. For the fixed-time responses, each column of X represents a
196 latency in ms before/after an experimental event; by contrast, for the scaled-time responses,
197 each column of X represents the *percentage* of time that has elapsed between *two* events
198 (stimulus and response). Simulation code is available at
199 https://git.fmrib.ox.ac.uk/chassall/temporal-scaling.

200 **Production and Perception Tasks**

201 ***Participants***

202 Participants completed both the production and perception tasks within the same
203 recording session. We tested ten university-aged participants, 5 male, 2 left-handed, M_{age} =
204 23.40, 95% CI [21.29, 25.51]. Participants had normal or corrected-to-normal vision and no
205 known neurological impairments. Participants provided informed consent approved by the
206 Medical Sciences Interdivisional Research Ethics Committee at the University of Oxford.
207 Following the experiment, participants were compensated £20 (£10 per hour of participation)
208 plus a mean performance bonus of £3.23, 95% CI [2.92, 3.55].

209 ***Apparatus and Procedure***

210 Participants were seated approximately 64 cm from a 27-inch LCD display (144 Hz, 1
211 ms response rate, 1920 by 1080 pixels, Acer XB270H, New Taipei City, Taiwan). Visual
212 stimuli were presented using the Psychophysics Toolbox Extension [49,50] for MATLAB
213 2014b (Mathworks, Natick, USA). Participants were given written and verbal instructions to
214 minimize head and eye movements. The goal of the production task was to produce a target
215 interval and the goal of the perception task was to judge whether or not a computer-produced
216 interval was correct.

217 The experiment was blocked with ten trials per block. There were 18 production
218 blocks and 18 perception blocks, completed in random order. Prior to each block, participants

listened to five isochronic tones indicating the target interval. Beeps were 400 Hz sine waves of duration 50 ms and an onset/offset ramping to a point 1/8 of the length of the wave (to avoid abrupt transitions). The target interval was either short (0.8 s), medium (1.65 s), or long (2.5 s).

In production trials, participants listened to a beep then waited the target time before responding. Feedback appeared after a 400-600 ms delay (uniform distribution) and remained on the display for 1000 ms. Feedback was a 'quarter-to' clockface to indicate 'too early', a 'quarter-after' clockface to indicate 'too late', or a checkmark to indicate an on-time response. Feedback itself was determined by where the participant's response fell relative to a window around the target duration. The response window was initialized to +/- 100 ms around each target, then changed following each feedback via a staircase procedure: increased on each side by 10 ms following a correct response and decreased by 10 ms following an incorrect response (either too early or too late).

In perception trials, participants heard two beeps, then were asked to judge the correctness of the interval, that is, whether or not the test interval matched the target interval. Test intervals (very early, early, on time, late, very late) were set such that each subsequent interval was 25% longer than the previous (see Supplementary Table 1). Participants were then given feedback on their judgement – a checkmark for a correct judgement, or an 'x' for an incorrect judgement.

For each task, participants gained 2 points for each correct response and lost 1 point for each incorrect response. At the end of the experiment points were converted to a monetary bonus at a rate of £0.01 per point.

Data Collection

In the perception task we recorded participant response time from cue, trial outcome (early, late, on time), and staircase- response window. In the production task, we recorded trial 'on time' judgements (yes/no), and trial outcome (correct/incorrect).

We recorded 36 channels of EEG, referenced to AFz. Data were recorded at 1000 Hz using a Synamps amplifier and CURRY 8 software (Compumetrics Neuroscan, Charlotte, USA). The electrodes were sintered Ag/AgCl (EasyCap, Herrsching, Germany). 31 of the electrodes were laid out according to the 10-20 system. Additional electrodes were placed on the left and right mastoids, on the outer canthi of the left and right eyes, and below the right eye. The reference electrode was placed at location AFz, and the ground electrode at Fpz.

Prediction Task

In this previously published [32,33] experiment, 19 participants responded to the onset of a visual target following a visual warning cue. The delay between cue and target was either short (700 ms) or long (1300 ms) and, in some conditions, congruent with a preceding stimulus stream. Only these predictable trials were included in the current analysis (i.e., the 'valid' trials in the 'Rhythmic' and 'Repeated-Interval' conditions – see [32,33] for more detail).

Decision-Making Task

In this experiment, also previously published [34,35], 18 participants were presented with two snack foods and asked to pick one. This was not an interval timing task and on average participants took 763 ms, 95% CI [713, 813], to respond.

Data Analysis

Behavioural data

For the perception task, we computed mean window size and mean produced interval for each participant. For the production task, we computed mean likelihood of responding yes

266 to the ‘on time’ prompt, for each condition (short, medium, long) and interval (very early,
267 early, on time, late, very late).

268 ***EEG Preprocessing***

269 For all three timing tasks, EEG was preprocessed in MATLAB 2020b (Mathworks,
270 Natick, USA) using EEGLAB [51]. We first down-sampled the EEG to 200 Hz, then applied
271 a 0.1-20 Hz bandpass filter and 50 Hz notch filter. The EEG was then re-referenced to the
272 average of the left and right mastoids (and AFz recovered in the production/perception tasks).
273 Ocular artifacts were removed using independent component analysis (ICA). The ICA was
274 trained on 3-second epochs of data following the appearance of the fixation cross at the
275 beginning of each trial. Ocular components were identified using the *iclabel* function and
276 then removed from the continuous data.

277 EEG for the decision-making task was already preprocessed prior to our analysis. This
278 was a simultaneous EEG-fMRI recording, and preprocessing included the removal of MR-
279 related artifacts via filtering and principal component analysis, as well as a 0.5-40 Hz
280 bandpass filter. In line with our other analyses, we re-referenced the EEG to the average of
281 TP7 and TP8 (located close to the mastoids) and applied an additional 20 Hz low-pass filter.

282 ***ERPs***

283 To construct conventional event-related potentials (ERPs), we first created epochs of
284 EEG around cues (all tasks), responses (perception task), probes (production task), targets
285 (prediction task), and decisions (decision-making task). Cue-locked ERPs extended from 200
286 ms pre-cue to either 800, 1650, or 2500 ms post-cue (the short, medium, and long targets) in
287 the perception/production tasks, 700 or 1300 ms in the prediction task (the short and long
288 targets), and 600 ms in the decision-making task. Epochs were baseline-corrected using a 200
289 ms pre-cue window. We also constructed epochs from 800, 1650, or 2500 ms prior to the
290 response/probe in the production/perception tasks, 700 or 1300 ms prior to the target in the

291 prediction task, and 600 prior to the decision in the decision-making task to 200 ms after the
292 response/probe/target/decision. A baseline was defined around the event of interest (mean
293 EEG from -20 to 20 ms) and removed in all cases except for the decision-making task, in line
294 with the original analysis [34]. We then removed any trials in which the sample-to-sample
295 voltage differed by more than 50 μV or the voltage change across the entire epoch exceeded
296 150 μV. We then created conditional cue and response/probe/target/decision averages for
297 each participant and task: production/perception (short, medium, and long), prediction (short
298 and long), and decision-making (early and late, via a median split [34]). Finally, participant
299 averages in the timing tasks were combined into grand-average waveforms at electrode FCz,
300 a location where timing-related activity has been previously observed [5] and Pz in the
301 decision-making task, in line with the previously published analysis [34] (Supplementary Fig
302 4).

303 ***rERPs***

304 To unmix fixed-time and scaled-time components in our EEG data, we estimated
305 regression-ERPs (rERPs) following the same GLM procedure we used with our simulated
306 data, but now applied to each sensor. We used a design matrix consisting of a regular stick
307 functions for cue and response/probe/target and a stretched/compressed stick function
308 spanning the interval from cue to response/probe/target/decision. In particular, we estimated
309 cue-locked responses that spanned from 200 ms pre-cue to 800 ms post-cue. The
310 response/probe/target/decision response interval spanned from -800 to 200 ms. Each fixed-
311 time response thus spanned 1000 ms, or 200 EEG sample points. The scaled-time component,
312 as described earlier, was modelled as a single underlying component (set width in X) that
313 spanned over multiple EEG durations (varying number of rows in X). Thus, our method
314 required choosing how many scaled-time sample points to estimate (the width in X). For the
315 production/perception tasks, we chose to estimate 330 scaled-time points, equivalent to the

duration of the ‘medium’ interval. For the prediction task, we chose to estimate 200 scaled-time points, equivalent to the mean of the short and long conditions (700 ms, 1300 ms). For the decision-making task, we estimated 153 scaled-time points (roughly equivalent to the mean decision time). Unlike the conventional ERP approach, this analysis was conducted on the continuous EEG. To identify artifacts in the continuous EEG, we used the *basicrap* function from the ERPLAB [52] toolbox with a 150 μV threshold (2000 ms window, 1000 ms step size). A sample was flagged if it was ‘bad’ for any channel. Flagged samples were excluded from the GLM (samples removed from the EEG and rows removed from the design matrix). Additionally, we removed samples/rows associated with unusually fast or slow responses in the production task (less than 0.2 s or more than 5 s). On average, we removed 2.17 % of samples in the production task (95% CI [1.49, 2.86]), 3.75 % of samples in the perception task (95% CI [2.39, 5.10]), 1.03% of samples in the prediction task (95% CI [0.95, 1.10]), and 5.56% of samples in the decision-making task (95% CI [4.99, 6.12]).

To impose a smoothness constraint on our estimates, we used a first-derivative form of Tikhonov regularization [29]. Tikhonov regularization reframes the GLM solution as the minimization of:

$$\|X\beta - \mathrm{Y}\|^2 + \lambda\|\mathrm{L}\beta\|^2$$

where L is the regularization operator and λ is the regularization parameter. In other words, we aimed to minimize a penalty term in addition to the usual residual. This has the solution

$$(X^T X + \lambda \mathrm{L})^{-1} X^T Y$$

In our case, L approximated the first derivative as a scaled finite difference[53]:

$$L = \frac{1}{2}\begin{bmatrix} 1 & -1 & 0 & \dots & 0 & 0 \\ 0 & 1 & -1 & \dots & 0 & 0 \\ \dots & \dots & \dots & \dots & \dots & \dots \\ 0 & 0 & 0 & \dots & 1 & -1 \end{bmatrix}$$

We then chose regularization parameters for each participant using 10-fold cross validation. Our goal here was to minimize the mean-squared error of the residual EEG at electrode FCz, our electrode of interest. The following λs were tested on each fold: 0.001, 0.01, 0, 1, 10, 100, 1000, 10000, 100000. An optimal λ was chosen for each participant corresponding to the parameter with the lowest mean mean-squared error across all folds. See Supplementary Table 4 for a summary.

Statistics

We quantified the amplitude of the scaled-time component in two ways. First, we computed and plotted the 95% confidence interval at each 'timepoint' of the scaled-time signal (right column of Fig 2). Next, we conducted a nonparametric statistical test of the scaled-time component according to the procedure outlined in [54]. After computing a single-sample *t*-statistic at each sample point, we identified clusters of points for with the *t*-value exceeded a critical threshold corresponding to an alpha level of .05 (i.e., the 2.5^{th} and 97.5^{th} percentiles, making this a two-sided test). For each cluster, we computed the 'cluster mass', defined as the sum of the absolute values of the *t*-values within the cluster. To determine whether the observed cluster masses exceeded what could occur by chance, we permuted the scaled components by randomly flipping (multiplying by -1) the entire waveform. We then computed the cluster masses for the permuted waveforms as before, and recorded the maximum cluster mass (or zero if there were no clusters). Every possible permutation was checked for the production and perception tasks (2^{10} = 1024 permutations). For the prediction and decision-making tasks, 1000 random permutations were checked. We then labelled our observed cluster masses as 'significant' if they exceeded 95% of the maximum cluster masses of the permuted waveforms. These analyses were done at the scalp location where the mean scaled-time signal reached its most negative value, i.e. electrode Cz in the production/perception tasks, FCz in the prediction task, and C1 in the decision-making task.

364 ***PCA***

365 To explore the link between the scaled-time component and behaviour, we regressed
366 out the fixed-time components from the EEG in the temporal production task – that is, we
367 reconstructed the preprocessed data using only the scaled-time regressors plus residuals. Only
368 mid-frontal electrodes were considered: FC1, FCz, FC2, Cz, CP1, CPz, and CP2. We then
369 constructed epochs starting at the cue and ending at the target interval (800 ms, 1650 ms, or
370 2500 ms). Epochs within each condition (short, medium, long) were further grouped into
371 three equal-sized response-time bins (early, on time, late) and averaged for each electrode
372 and participant. We then conducted a PCA for each condition (short, medium, long) and
373 participant. See Supplementary Table 2 for amount of variance explained by PC1 and PC2.
374 To visualize the effect of PC2, we computed the mean PC2 across all participants. We then
375 added more or less of the mean PC2 to the mean PC1 projection and applied a 25-point
376 moving-mean window for visualization purposes (Supplementary Fig 5). In order to choose a
377 reasonable range of PC2 scores, we examined the average minimum and maximum PC2
378 score for each participant and condition (short, medium, long). The PC2 score ranges were -
379 21 to 15 (short), -41 to 38 (medium), and -40 to 55 (long). To assess the relationship between
380 PC2 score and behaviour, we binned PC2 scores according to our response time bins (early,
381 on time, late) and collapsed across conditions (short, medium, long). This gave us as single
382 mean PC2 score for each participant and response time bin (early, on time, late), which we
383 analyzed using a two-sided repeated-measures ANOVA (Fig 3d) after verifying the
384 assumption of normality using the Shapiro-Wilk test. Two different effect sizes, η_p^2 and η_g^2,
385 were computed, according to:

386 $$\eta_p^2 = \frac{SS_Q}{SS_Q + SS_{sQ}} \qquad \eta_g^2 = \frac{SS_Q}{SS_Q + SS_S + SS_{sQ}}$$

387 where SS_Q is the sum of squares of the quantile effect (early, on time, late), SS_{sQ} is the error
388 sum of squares of the quantile effect, and SS_S is the sum of squares between subjects [55].

We then replicated the PCA procedure for the decision-making task using an epoch extending 800 ms from the cue at a central electrode cluster (FC3, FC1, FC2, FC4, C3, C1, Cz, C2, C4, CP3, CP1, CP2, CP4, P3, P1, Pz, P2, and P4). Note that the assumption of normality was violated for ‘early' responses in the decision-making task. However, as repeated-measures ANOVA is robust to violations of normality, no statistical correction was made.

Data Availability

Raw and preprocessed EEG for the production and perception tasks will be made publicly available at the time of publication. Raw data for the prediction task is available at https://doi.org/10.5061/dryad.5vb8h. Raw data for the decision-making task is available at https://openneuro.org/datasets/ds002734/versions/1.0.2.

Code Availability

Simulation and analysis scripts are available athttps://git.fmrib.ox.ac.uk/chassall/temporal-scaling.

References

1. Bogacz R, Brown E, Moehlis J, Holmes P, Cohen JD. The Physics of Optimal Decision Making: A Formal Analysis of Models of Performance in Two-Alternative Forced-Choice Tasks. Psychological Review. 113: 700–765.

2. Merchant H, Harrington DL, Meck WH. Neural Basis of the Perception and Estimation of Time. Annu Rev Neurosci. 2013;36: 313–336. doi:10.1146/annurev-neuro-062012-170349

3. Wittmann M. The inner sense of time: how the brain creates a representation of duration. Nature Reviews Neuroscience. 2013;14: 217–223. doi:10.1038/nrn3452

4. Nobre AC, van Ede F. Anticipated moments: temporal structure in attention. Nature Reviews Neuroscience. 2018;19: 34–48. doi:10.1038/nrn.2017.141

5. Macar F, Vidal F. Event-Related Potentials as Indices of Time Processing: A Review. Journal of Psychophysiology. 2004;18: 89–104. doi:10.1027/0269-8803.18.23.89

6. Kononowicz TW, van Rijn H. Decoupling Interval Timing and Climbing Neural Activity: A Dissociation between CNV and N1P2 Amplitudes. J Neurosci. 2014;34: 2931–2939. doi:10.1523/JNEUROSCI.2523-13.2014

7. Pfeuty M, Ragot R, Pouthas V. Relationship between CNV and timing of an upcoming event. Neuroscience Letters. 2005;382: 106–111. doi:10.1016/j.neulet.2005.02.067

8. Macar F, Vidal F, Casini L. The supplementary motor area in motor and sensory timing: evidence from slow brain potential changes. Exp Brain Res. 1999;125: 271–280. doi:10.1007/s002210050683

9. Trillenberg P, Verleger R, Wascher E, Wauschkuhn B, Wessel K. CNV and temporal uncertainty with 'ageing' and 'non-ageing' S1–S2 intervals. Clinical Neurophysiology. 2000;111: 1216–1226. doi:10.1016/S1388-2457(00)00274-1

10. Miniussi C, Wilding EL, Coull JT, Nobre AC. Orienting attention in time: Modulation of brain potentials. Brain. 1999;122: 1507–1518. doi:10.1093/brain/122.8.1507

11. Macar F, Vidal F. The CNV peak: An index of decision making and temporal memory. Psychophysiology. 2003;40: 950–954. doi:10.1111/1469-8986.00113

12. Praamstra P, Kourtis D, Kwok HF, Oostenveld R. Neurophysiology of Implicit Timing in Serial Choice Reaction-Time Performance. J Neurosci. 2006;26: 5448–5455. doi:10.1523/JNEUROSCI.0440-06.2006

13. Macar F, Vidal F. Time processing reflected by EEG surface Laplacians. Exp Brain Res. 2002;145: 403–406. doi:10.1007/s00221-002-1103-z

14. Walter WG, Cooper R, Aldridge VJ, McCallum WC, Winter AL. Contingent Negative Variation : An Electric Sign of Sensori-Motor Association and Expectancy in the Human Brain. Nature. 1964;203: 380–384. doi:10.1038/203380a0

15. Wang J, Narain D, Hosseini EA, Jazayeri M. Flexible timing by temporal scaling of cortical responses. Nat Neurosci. 2018;21: 102–110. doi:10.1038/s41593-017-0028-6

16. Remington ED, Egger SW, Narain D, Wang J, Jazayeri M. A Dynamical Systems Perspective on Flexible Motor Timing. Trends in Cognitive Sciences. 2018;22: 938–952. doi:10.1016/j.tics.2018.07.010

17. Vyas S, Golub MD, Sussillo D, Shenoy KV. Computation Through Neural Population Dynamics. Annual Review of Neuroscience. 2020;43: 249–275. doi:10.1146/annurev-neuro-092619-094115

18. Sussillo D. Neural circuits as computational dynamical systems. Current Opinion in Neurobiology. 2014;25: 156–163. doi:10.1016/j.conb.2014.01.008

19. Williams AH, Poole B, Maheswaranathan N, Dhawale AK, Fisher T, Wilson CD, et al. Discovering Precise Temporal Patterns in Large-Scale Neural Recordings through Robust and Interpretable Time Warping. Neuron. 2020;105: 246-259.e8. doi:10.1016/j.neuron.2019.10.020

20. O'Connell RG, Shadlen MN, Wong-Lin K, Kelly SP. Bridging Neural and Computational Viewpoints on Perceptual Decision-Making. Trends in Neurosciences. 2018;41: 838–852. doi:10.1016/j.tins.2018.06.005

21. Boehm U, van Maanen L, Forstmann B, van Rijn H. Trial-by-trial fluctuations in CNV amplitude reflect anticipatory adjustment of response caution. Neuroimage. 2014;96: 95–105. doi:10.1016/j.neuroimage.2014.03.063

22. Meck WH. Neuropsychology of timing and time perception. Brain and Cognition. 2005;58: 1–8. doi:10.1016/j.bandc.2004.09.004

23. Luck SJ. A Closer Look at ERPs and ERP Components. Second edition. An introduction to the event-related potential technique. Second edition. Cambridge, Massachusetts: The MIT Press; 2014. pp. 35–70.

24. Smith NJ, Kutas M. Regression-based estimation of ERP waveforms: I. The rERP framework. Psychophysiology. 2015;52: 157–168. doi:10.1111/psyp.12317

25. Ehinger BV, Dimigen O. Unfold: an integrated toolbox for overlap correction, non-linear modeling, and regression-based EEG analysis. PeerJ. 2019;7: e7838. doi:10.7717/peerj.7838

26. Litvak V, Jha A, Flandin G, Friston K. Convolution models for induced electromagnetic responses. Neuroimage. 2013;64: 388–398. doi:10.1016/j.neuroimage.2012.09.014

27. Lalor EC, Pearlmutter BA, Reilly RB, McDarby G, Foxe JJ. The VESPA: A method for the rapid estimation of a visual evoked potential. NeuroImage. 2006;32: 1549–1561. doi:10.1016/j.neuroimage.2006.05.054

28. Crosse MJ, Di Liberto GM, Bednar A, Lalor EC. The Multivariate Temporal Response Function (mTRF) Toolbox: A MATLAB Toolbox for Relating Neural Signals to Continuous Stimuli. Front Hum Neurosci. 2016;10. doi:10.3389/fnhum.2016.00604

29. Kristensen E, Guerin-Dugué A, Rivet B. Regularization and a general linear model for event-related potential estimation. Behav Res. 2017;49: 2255–2274. doi:10.3758/s13428-017-0856-z

30. Wiener M, Kanai R. Frequency tuning for temporal perception and prediction. Current Opinion in Behavioral Sciences. 2016;8: 1–6. doi:10.1016/j.cobeha.2016.01.001

31. Herrmann CS, Rach S, Vosskuhl J, Strüber D. Time–Frequency Analysis of Event-Related Potentials: A Brief Tutorial. Brain Topogr. 2014;27: 438–450. doi:10.1007/s10548-013-0327-5

32. Breska A, Deouell LY. Neural mechanisms of rhythm-based temporal prediction: Delta phase-locking reflects temporal predictability but not rhythmic entrainment. PLOS Biology. 2017;15: e2001665. doi:10.1371/journal.pbio.2001665

33. Breska A, Deouell LY. Data from: Neural mechanisms of rhythm-based temporal prediction: delta phase-locking reflects temporal predictability but not rhythmic entrainment. 2017. doi:doi:10.5061/dryad.5vb8h

34. Pisauro MA, Fouragnan E, Retzler C, Philiastides MG. Neural correlates of evidence accumulation during value-based decisions revealed via simultaneous EEG-fMRI. Nat Commun. 2017;8: 1–9. doi:10.1038/ncomms15808

35. Pisauro MA, Fouragnan E, Retzler C, Philiastides MG. Evidence Accumulation in Value-Based decisions. 2020. doi:10.18112/openneuro.ds002734.v1.0.2

36. Krajbich I, Armel C, Rangel A. Visual fixations and the computation and comparison of value in simple choice. Nature Neuroscience. 2011;13: 10.

37. Luck SJ. An introduction to the event-related potential technique. Second edition. Cambridge, Massachusetts: The MIT Press; 2014.

38. Möcks J. The Influence of Latency Jitter in Principal Component Analysis of Event-Related Potentials. Psychophysiology. 1986;23: 480–484. doi:10.1111/j.1469-8986.1986.tb00659.x

39. Hunt LT, Behrens TE, Hosokawa T, Wallis JD, Kennerley SW. Capturing the temporal evolution of choice across prefrontal cortex. Frank MJ, editor. eLife. 2015;4: e11945. doi:10.7554/eLife.11945

40. Ariely D, Zakay D. A timely account of the role of duration in decision making. Acta Psychologica. 2001;108: 187–207. doi:10.1016/S0001-6918(01)00034-8

41. O'Connell RG, Dockree PM, Kelly SP. A supramodal accumulation-to-bound signal that determines perceptual decisions in humans. Nature Neuroscience. 2012;15: 1729–1735. doi:10.1038/nn.3248

42. Kelly SP, O'Connell RG. Internal and External Influences on the Rate of Sensory Evidence Accumulation in the Human Brain. Journal of Neuroscience. 2013;33: 19434–19441. doi:10.1523/JNEUROSCI.3355-13.2013

43. Kösem A, Bosker HR, Takashima A, Meyer A, Jensen O, Hagoort P. Neural Entrainment Determines the Words We Hear. Current Biology. 2018;28: 2867-2875.e3. doi:10.1016/j.cub.2018.07.023

44. Abrams DA, Nicol T, Zecker S, Kraus N. Abnormal Cortical Processing of the Syllable Rate of Speech in Poor Readers. J Neurosci. 2009;29: 7686–7693. doi:10.1523/JNEUROSCI.5242-08.2009

45. Müller JA, Wendt D, Kollmeier B, Debener S, Brand T. Effect of Speech Rate on Neural Tracking of Speech. Front Psychol. 2019;10. doi:10.3389/fpsyg.2019.00449

46. Lerner Y, Honey CJ, Katkov M, Hasson U. Temporal scaling of neural responses to compressed and dilated natural speech. Journal of Neurophysiology. 2014;111: 2433–2444. doi:10.1152/jn.00497.2013

47. Allman MJ, Meck WH. Pathophysiological distortions in time perception and timed performance. Brain. 2012;135: 656–677. doi:10.1093/brain/awr210

48. Smith NJ, Kutas M. Regression-based estimation of ERP waveforms: II. Nonlinear effects, overlap correction, and practical considerations. Psychophysiology. 2015;52: 169–181. doi:10.1111/psyp.12320

49. Brainard DH. The psychophysics toolbox. Spatial vision. 1997;10: 433–436.

50. Pelli DG. The VideoToolbox software for visual psychophysics: transforming numbers into movies. Spatial Vision. 1997;10: 437–442. doi:10.1163/156856897X00366

51. Delorme A, Makeig S. EEGLAB: an open source toolbox for analysis of single-trial EEG dynamics including independent component analysis. Journal of Neuroscience Methods. 2004;134: 9–21. doi:10/bqr2f2

52. Lopez-Calderon J, Luck SJ. ERPLAB: an open-source toolbox for the analysis of event-related potentials. Front Hum Neurosci. 2014;8. doi:10.3389/fnhum.2014.00213

53. Reichel L, Ye Q. Simple Square Smoothing Regularization Operators. Electronic Transactions on Numerical Analysis. 2008;33: 63–83.

54. Maris E, Oostenveld R. Nonparametric statistical testing of EEG- and MEG-data. Journal of Neuroscience Methods. 2007;164: 177–190. doi:10.1016/j.jneumeth.2007.03.024

55. Olejnik S, Algina J. Generalized eta and omega squared statistics: measures of effect size for some common research designs. Psychol Methods. 2003;8: 434–447. doi:10.1037/1082-989X.8.4.434